Optical absorption of polydisperse TiO_2: Effect of surface doping by transition metal cations

[1] Kernazhitsky L., [1] Shymanovska V., [1] Gavrilko T., [1] Naumov V. and [2] Kshnyakin V.

[1] Institute of Physics, National Academy of Sciences of Ukraine, 46 Nauky Ave., 03028 Kyiv, Ukraine, E-mail: kern@iop.kiev.ua
[2] Sumy State University, 2 Rymsky-Korsakov St., 40007 Sumy, Ukraine

Received: 24.10.2012

Abstract. We have investigated the effect of doping of nanocrystalline TiO_2 with transition metal cations (Cu^{2+}, Fe^{3+}, Co^{2+} and Cr^{3+}) on the properties related to optical absorption. The metal-doped TiO_2 samples obtained by us have been characterised using an X-ray diffractometry, X-ray fluorescence analysis, a scanning electron microscopy, and a UV–visible absorption spectroscopy. It has been shown that the doping effects on the properties of anatase and rutile are quite different, being much stronger and complicated in the case of anatase. The anatase doped with Fe and Cr cations reveals a 'red' shift of the absorption edge and narrowing of the bandgap.

Keywords: titanium dioxide, transition metals, bandgap, UV and visible optical absorption

PACS: 61.72.Uj, 71.55.Eq, 78.40.Fy
UDC: 535.3

1. Introduction

Titanium dioxide (TiO_2) is a photoactive semiconductor widely used in photocatalysis, photovoltaics, photonics, and photosensors [1–3]. However, large enough bandgap of TiO_2 allows its photonic activation only under exposure with the UV light (the wavelengths $\lambda < 380$ nm), thus limiting possible applications, e.g., in the photocatalysis occurring under natural solar irradiation [4]. A lot of work has been done on doping TiO_2 with various metal cations aimed at changing its electronic and optical properties in order to make the material more sensitive and extend its spectral response towards the visible spectral range. Nonetheless, it is difficult to make a direct comparison of the results of different authors due to varied experimental conditions, preparation techniques and sample testing methods. Up to now, the topic remains a subject of extensive studies and discussions [1, 5]. In most cases, the decisive factors of discrepancies among the results of different authors are the initial conditions of TiO_2 synthesis, terms and parameters of thermal and chemical treatment, crystal structure of the starting compound, particle sizes and dispersions, and, finally, a type and a concentration of dopants influencing the properties of TiO_2.

To clarify the role of transition-metal impurities on the optical properties of pure and doped TiO_2, in this work we perform comparative studies of optical absorption for a pure and surface-doped anatase and rutile in the region of photon energies $h\nu = 1.7–5.5$ eV.

2. Experimental

2.1. Preparation of samples and experimental methods

Samples of single-phase rutile (*R*) and anatase (*A*) structures of TiO_2 were synthesised by thermal hydrolysis of titanium tetrachloride hydrochloric acid solutions, according to the procedure de-

scribed earlier in the work [6]. Then the pure TiO_2 samples were chemically modified with selected transition-metal cations (Cu^{2+}, Fe^{2+}, Co^{2+} and Cr^{3+}), using adsorption from aqueous solutions of the appropriate sulphates ($CuSO_4$ and $FeSO_4$) or chlorides ($CrCl_3$ and $CoCl_2$). The sediment obtained was filtered, dried at 150°C for 5 h, carefully washed with bi-distilled water until the impurities disappeared in the filtrate, then calcined at 300°C in the open air for 8 h, and finally cooled down to the room temperature. It is worth noticing that all the impurity cations were adsorbed on the surface of the same initial anatase or rutile TiO_2 materials.

The structural properties and the phase compositions of thus synthesised TiO_2 samples were determined with an X-ray diffractometric (XRD) technique, using a DRON-2 diffractometer with $Cu_{K\alpha}$ (λ = 1.5406 Å) and $Co_{K\alpha}$ (λ = 1.7902 Å) radiations. The average crystallite sizes of the anatase and rutile TiO_2 were evaluated from the *A*(101) and *R*(110) diffraction peak widths, using a known Debye–Scherer formula. The chemical composition of TiO_2 samples was determined with the aid of an X-ray fluorescence (XRF) analysis, using an XNAT-Control instrument. The surface morphology and the impurity distribution were analysed by a scanning electron microscopy (SEM), using an apparatus JEOL JSM 6490 equipped with an X-ray energy-dispersive spectrometer (EDS) operating at 20 kV. The measurement errors for the XRF and EDS data did not exceed ±5% and ±10%, respectively.

The optical absorption spectra for our TiO_2 samples were measured in both the UV and visible spectral ranges (λ = 220–750 nm), using a multi-channel optical spectral analyser SL40-2 (TCD1304AP 3648-pixel CCD sensor, the diffraction grating 600 mm^{-1}, the spectral resolution ~ 0.3 nm, and the registration time ~ 7 ms). A deuterium lamp DDC-30 ($\lambda_{1\,max}$ = 245 nm, $\lambda_{2\,max}$ = 11 nm) and a xenon lamp DKSH-1000 (λ_{max} = 472 nm) were used as light sources. The samples for optical studies were prepared using a KBr pellet technique, with the TiO_2/KBr ratio being ~ 0.1 % wt. All the measurements were carried out at the room temperature.

3. Results and discussion

3.1. SEM and XRD analysis

According to the SEM data, the pure TiO_2 particles, of the both types *A* and *R*, synthesised by us are of nearly spherical shape, ranging from 5 to 10 μm in size. They consist of aggregated nanocrystallites. The average sizes of nanocrystallites in the polydisperse TiO_2 powders have been determined from the XRD patterns under the $Cu_{K\alpha}$ irradiation. They are equal to 10–36 and 8–16 nm for the *R* and *A* samples, respectively (see Table 1).

Table 1. Dopant concentrations and average crystallite sizes (D_{hkl}) of TiO_2 samples.

Sample	Dopant concentration, at. % (XRF)	Dopant concentration, at. % (EDS)	Average crystallite size (±3nm), nm (XRD)
Pure *R*	–	–	21
R/Cu	4.5	4.6	10
R/Co	2.4	1.1	29
R/Fe	2.2	3.5	15
R/Cr	1.0	2.3	36
Pure *A*	–	–	16
A/Cu	5.7	–	8
A/Co	3.3	–	13
A/Fe	2.6	–	9
A/Cr	2.6	–	15

3.2. XRF and EDS analyses

The contents of impurities in the doped TiO_2 samples have been evaluated with the XRF and EDS techniques and the impurity distribution over the TiO_2 surface has been determined from the EDS. The EDS data (the contents of Ti, O and the impurity atoms on the sample surface) have been obtained using a microprobe analysis at different points at the TiO_2 surface. It is worth noticing that, while the XRF results are linked to the total amount of Ti atoms only, the EDS data are based on the total amounts of Ti, O and the impurity atoms. Therefore, for proper comparison with the EDS data, the XRF results have been converted to the total amounts of different atoms in the TiO_2 samples (see Table 1).

3.3. UV–visible absorption spectra

As already mentioned, the absorption spectra of our TiO_2 samples have been studied in the range of photon energies 1.7–5.5 eV, which covers both the UV and visible ranges (750–220 nm). In the region of 1.7–3.1 eV corresponding to the energies less than the absorption edge energy, the intrinsic absorption bands of the impurity ions are superimposed with the absorption peaks of the undoped TiO_2 (see Fig. 1). The two absorption bands of the rutile samples centred at 3.03 eV and 3.05 eV (see Fig. 1a) are associated respectively with dipole-allowed $2p_{xy}$ exciton transitions and phonon-assisted indirect transitions. The authors of the work [7] assign the band located at 3.049 eV to an indirect bandgap transition. Usually, these bands are detected in the rutile crystals only at low temperatures. For the first time we have observed these features at the room temperature. This applies not only to the undoped rutile, but also to the anatase TiO_2 powders (see Fig. 2b). A weak absorption with sharp structure at 3.01 eV has not previously been observed at the room temperature. It may be attributed to a direct forbidden transition Γ_3–Γ_1 [8].

Several absorption bands with prominent peaks centred at 2.85, 2.91, 2.92, 2.93 and 2.96 eV are observed for all TiO_2 samples near the absorption edge (2.8–3.0 eV). As seen from Fig. 1, doping of the *R* samples does not lead to noticeable changes in the positions or the intensities of these absorption bands, whereas the absorption band intensities for the doped *A* samples decrease, depending on the doping elements. This decrease may be represented by a conventional sequence *A* > *A*/Cr > *A*/Fe > *A*/Co > *A*/Cu (see Fig. 1b).

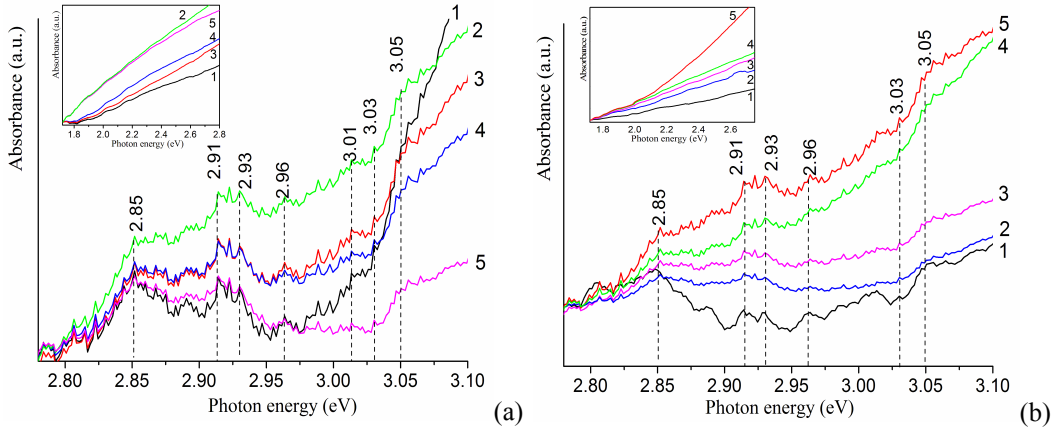

Fig. 1. UV–visible absorption spectra for pure and doped rutile (a) and anatase (b) TiO_2 samples in the region of 2.8–3.1 eV: (a) *R* (1), *R*/Fe (2), *R*/Cr (3), *R*/Cu (4), and *R*/Co (5); (b) *A* (1), *A*/Cu (2), *A*/Co (3), *A*/Fe (4), and *A*/Cr (5). Inserts show absorption spectra in the spectral region of 1.7–2.8 eV.

In general, there are two major factors determining the occurrence of the above-mentioned peaks in the absorption spectra of TiO_2 samples. First, it is an electron transfer from oxygen (O^{2-})

to titanium (Ti^{4+}) ions, resulting in formation of excitons. Similar peaks have been observed in the photoluminescence spectra of anatase TiO_2 powder anchored onto porous Vycor glass [9] and in the rutile single crystals at low temperatures [10]. The authors of [9] have attributed these bands to vibrational structure, suggesting that the photon energy absorbed by TiO_2 is mainly localised at Ti–O bonds.

The second factor is associated with the existence of defect levels inside the bandgap. Closely located bands centred at 2.95 eV (420 nm) and 2.75 eV (450 nm) have earlier been observed by Ghosh et al. [11] under thermal excitation of the rutile single crystals. Khomenko et al. [12] have also observed weak absorption bands between 2.3 eV and 2.9 eV and assigned them to *d–d* transitions associated with Ti^{3+} localised states. These weak optical absorption bands may also be assigned to electron transitions from different trapping levels associated with oxygen vacancies [13].

The optical absorption linked with the pure TiO_2 is small in the range of 1.7–2.8 eV (see Fig. 1, inserts). The observed increase in the absorption for the doped TiO_2 can be caused by additional impurity states formed inside the bandgap [14, 15]. There is a correlation between the absorption and the concentration of dopants. For instance, the enhanced absorption observed for the *A*/Cr sample, contrary to the *R*/Cr sample, results from higher Cr^{3+} concentrations in the former sample (2.6 at. % against 1.0 at. % for *R*/Cr).

Fig. 2 shows the absorption spectra of our TiO_2 samples in the region of 3.0–5.5 eV, where the photon energy exceeds the absorption edge energy. The undoped anatase shows an exponential absorption edge which is much less steeper than that of rutile. Such slower exponential growth of the absorption edge in the anatase crystal, when compared with that of the rutile, has been observed at low temperatures in the study [16] and attributed to self-trapping of excitons, a presence of more defects, and a stronger dispersion at the conduction band minimum.

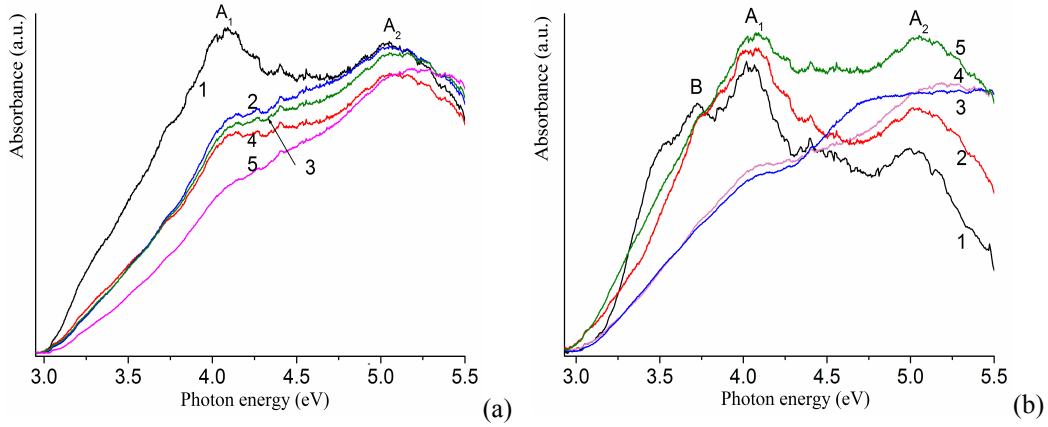

Fig. 2. UV–visible absorption spectra for pure and doped rutile (a) and anatase (b) TiO_2 samples in the region of 2.8–5.5 eV: (a) *R* (1), *R*/Cu (2), *R*/Fe (3), *R*/Cr (4), and *R*/Co (5); (b) *A* (1), *A*/Cr (2), *A*/Cu (3), *A*/Co (4), and *A*/Fe (5).

As seen from Fig. 2, the influence of dopants on the absorption in rutile is weaker than in anatase. No 'red' shift of the absorption edge has been observed for all of the doped *R* samples. This can be explained by the fact that rutile has a more compact structure when compared to anatase, which prevents penetration of the doping cations into the rutile lattice.

In contrast to the rutile, the doped *A*/Cr and *A*/Fe samples exhibit a 'red-shifted' absorption edge, though no such shift is observed for *A*/Cu and *A*/Co. According to [4], the 'red' shift of the

absorption edge in the anatase can be imposed by strong long-distance interaction of the transition-metal ions with the TiO_2 lattice.

It is easily seen that some spectral features in the region of 2.8–5.5 eV are similar for both the *A* and *R* structures. So, two characteristic absorption bands labelled as A_1 and A_2 are observed for the both structures. These bands correspond to the known absorption bands of TiO_2 single crystals, which have been thoroughly measured [17] and interpreted [18]. The A_1 and A_2 bands in the absorption spectrum of the pure rutile centred at 4.1 and 5.1 eV (see Fig. 2a) are attributed to splitting of O $2p_{x,y}$ orbitals in the valence band (VB). The first band A_1 is assigned to transitions between the top of the VB and the bottom of the conduction band (CB), and the second band A_2 is attributed to transitions between the top four states of the VB and the bottom six t_{2g} states of the CB [19].

The positions of the A_1 and A_2 bands in the absorption spectrum of the undoped anatase (see Fig. 2b) are similar to those observed in the rutile. An additional band for the anatase single crystals, which is centred at about 3.7 eV (labelled as *B*), has been for the first time observed in the work [20]. Asahi et al. [21] have assigned this band to a direct exciton transition from non-bonding O p_π states located at the top of the VB to non-bonding d_{xy} states located at the bottom of the CB.

As seen from Fig. 2, the influence of dopants on the *A* and *R* samples is rather different. In the case of rutile, the doping results in considerably decreasing intensity of the absorption band A_1 and, at the same time, it has little effect on the band A_2. From the other hand, the doping effect in the anatase is more complicated, causing changes in the relative intensities of both the A_1 and A_2 bands. The intensity of the A_2 band for all of the doped *A* samples is higher than that for the pure anatase.

In the case of *A*/Cu samples (see Fig. 2b), an enhanced absorption and a strong broadening of the absorption band A_2 (a plateau extending over the region of 4.4–5.5 eV) could be attributed to contribution from the intrinsic absorption of Cu cations (2.81–3.87 eV). According to [22], this band is probably related to overlapping charge transfer transitions $O^{2-}(2p) \rightarrow Ti^{4+}(3d)$ and $O^{2-}(2p) \rightarrow Cu^{2+}(3d)$.

3.4. Bandgap

The forbidden energy gap E_g for semiconductors is linked to the optical absorption coefficient α via the following relation [23]:

$$A_c(h\nu - E_g)^r = \alpha h\nu, \tag{1}$$

where $h\nu$ is the photon energy, A_c the constant associated with ordered crystalline structure, and *r* the exponent depending on the type of optical transitions. In particular, one has $r = 2$ for indirect-allowed transitions, 3/2 for direct-forbidden transitions, and 1/2 for direct-allowed transitions. Using Eq. (1), we have evaluated the bandgap values for our TiO_2 samples from the intersections of tangents to the curves $(\alpha h\nu)^{1/r}$ and the photon energy $h\nu$ axis, as illustrated in Fig. 3 and Fig. 4.

Fig. 3 shows the dependences $(\alpha h\nu)^{1/r}$ versus $h\nu$ obtained for both the doped and pure *R* samples. It is known for the rutile single crystals that the extended absorption edge is formed by the two mechanisms: the lower edge at 3.03–3.05 eV corresponds to direct-forbidden transitions Γ_3–Γ_1 [24] and the upper edge at 3.05–3.12 eV is attributed to indirect-allowed transitions X_2–Γ_1 [25]. A dotted rectangle in Fig. 3 outlines the region of direct-forbidden and indirect-allowed transitions in the rutile.

The direct bandgap value derived for the pure *R* sample equals to $E_{gd} = 3.01$ eV. This value agrees well with the data reported in [26] for the rutile single crystals. According to our measurements, the direct bandgap values for the doped *R* samples are practically the same as those for the

pure rutile (see Table 2). This correlates well with *ab initio* calculations by Karvinen et al. [27], where no bandgap narrowing has been obtained for the transition-metal doped rutile structure.

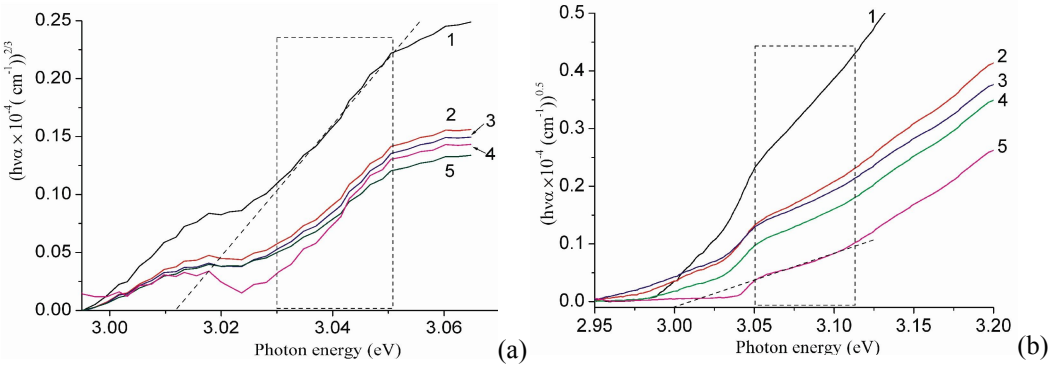

Fig. 3. Plots $(\alpha hv)^{1/r}$ versus hv (solid lines) for pure (a) and doped (b) TiO_2 rutile: (a) r = 3/2: *R* (1), *R*/Cr (2), *R*/Cu (3), *R*/Co (4), and *R*/Fe (5); (b) r = 2: *R* (1), *R*/Cr (2), *R*/Cu (3), *R*/Fe (4), and *R*/Co (5).

Table 2. Bandgap values for pure and doped anatase and rutile TiO_2 samples*.

Sample	E_{gd}, eV $r = 0.5$	E_{gi}, eV $r = 2$	Sample	E_{gd}, eV $r = 1.5$	E_{gi}, eV $r = 2$
A	3.25	3.08	*R*	3.01	2.97
A/Cu	3.21	2.97	*R*/Cu	3.02	2.93
A/Co	3.20	2.94	*R*/Co	3.03	2.99
A/Fe	3.13	2.96	*R*/Fe	3.02	2.83
A/Cr	3.14	2.94	*R*/Cr	3.02	2.91

* E_{gd} and E_{gi} denote bandgaps referred respectively to direct and indirect transitions (the errors are ±0.01 eV), and r is the exponent depending on the type of transitions.

It is known that the band structure of the anatase single crystals has two maxima, M and Γ, near the top of the VB, which are separated by a very small energy difference (~ 2 meV) [28]. The transitions from these states to the bottom of the CB can be either direct (Γ (VB) → Γ (CB)) [24] or indirect (M (VB) → Γ (CB)) [28]. This depends upon the crystalline structure, the lattice parameters, and the material dispersion. Thus, although the bulk TiO_2 belongs to indirect bandgap semiconductors, the nanostructured TiO_2 can reveal some properties of direct-bandgap semiconductors [29]. These two different kinds of transitions can be distinguished by the energy dependence of the corresponding absorption edge. To establish the type of the bandgap transitions which occur in the anatase samples synthesised here, we have fitted the experimental absorption spectra to Eq. (1), using the exponent values $r = 2$ and $r = 1/2$ for the indirect-allowed and direct-allowed transitions, respectively.

The dependences $(\alpha hv)^{1/r}$ versus (hv) obtained for the pure and doped *A* samples are shown in Fig. 4a and Fig. 4b, respectively. While extrapolating the linear part of the curve $(\alpha hv)^{1/2}$ versus hv for the pure anatase (see Fig. 4a), we have obtained the indirect bandgap 2.92 eV, which is in good compliance with the calculated value (2.91 eV [25]) corresponding to the indirect interband transition $X_{1a} \rightarrow G_{1b}$. Linear relationships have also been obtained when the absorption curves are fitted with the function $(\alpha hv)^2$ (see Fig. 4b). The absorption region marked with dotted rectangular in Fig. 4b is attributed to direct-allowed band transitions. For the undoped anatase, extrapolation of the linear part of the curve $(\alpha hv)^2$ versus (hv) gives a direct bandgap 3.29 eV, which is very close to the experimental value 3.3 eV found for the anatase single crystals [30], whereas the calculated bandgap value corresponding to the direct interband transition $X_{1a} \rightarrow C_{1b}$ is equal to 3.45 eV [31].

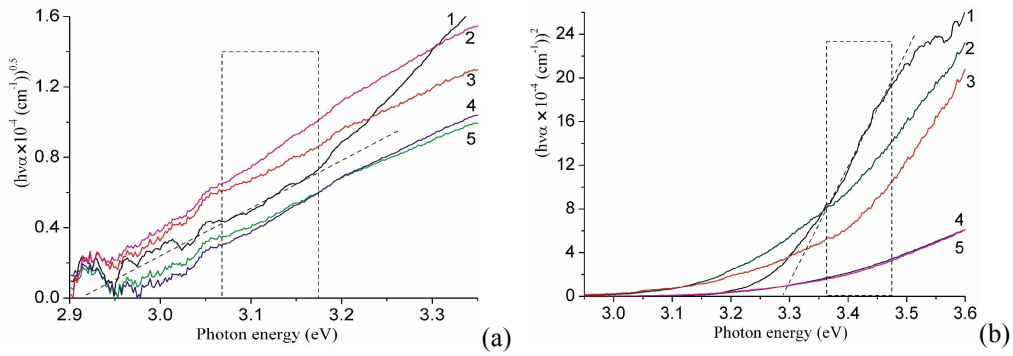

Fig. 4. Plots $(\alpha hv)^{1/r}$ versus hv (solid lines) for pure (a) and doped (b) anatase TiO_2: (a) $r = 2$: *A* (1), *A*/Co (2), *A*/Cr (3), *A*/Cu (4), and *A*/Fe (5); (b) $r = 1/2$: *A* (1), *A*/Fe (2), *A*/Cr (3), *A*/Cu (4), and *A*/Co (5).

The bandgap values obtained for the direct (E_{gd}) and indirect (E_{gi}) transitions for all of our TiO_2 samples are summarised in Table 2. One can see that the direct bandgap values for the doped anatase are smaller than those for the pure anatase (3.29 eV), being the smallest for the *A*/Cr (~ 3.14 eV) and *A*/Fe (~ 3.17 eV) samples. The direct bandgaps for *A*/Fe and *A*/Co are close to the values reported in the study [29]. Narrowing of the indirect bandgap observed for *A*/Cr and *A*/Cu is also similar to the effect found in [32] for the samples prepared with the other methods.

4. Conclusions

In the present work we have studied the optical absorption of polydisperse nanocrystalline rutile and anatase TiO_2 doped with metal cations (Cu^{2+}, Fe^{3+}, Co^{2+} and Cr^{3+}) under identical experimental conditions. The main portion of the absorption observed at 1.7–2.8 eV is defined by the states of doping metal cations, which are formed in the bandgap. The absorption peaks found at 2.8–3.0 eV are related to existence of defect levels and oxygen vacancies in the bandgap of TiO_2. The influence of dopants on the absorption of rutile in the region of 3.0–5.5 eV is smaller, when compared to anatase. It is shown that the bandgap of rutile does not change upon doping, though it narrows significantly for the doped anatase, being the narrowest for the *A*/Cr and *A*/Fe samples.

References

1. Henderson M A, 2011. A surface science perspective on TiO_2 photocatalysis. Surf. Sci. Rep. **66**: 185–297.
2. Fujishima A, Zhang X and Tryk D A, 2008. TiO_2 photocatalysis and related surface phenomena. Surf. Sci. Rep. **63**: 515–582.
3. Diebold U, 2003. The surface science of titanium dioxide. Surf. Sci. Rep. **48**: 53–229.
4. Anpo M, 2000. Use of visible light. Second-generation titanium oxide photocatalysts prepared by the application of an advanced metal ion-implantation method. Pure Appl. Chem. **72**: 1787–1792.
5. Takeuchi M, Matsuoka M and Anpo M, 2012. Ion engineering techniques for the preparation of the highly effective TiO_2 photocatalysts operating under visible light irradiation. Res. Chem. Intermed. **38**: 1261–1277.
6. Shimanovskaya V V, Dvernyakova A A and Strelko V V, 1988. The kinetics of the hydrolysis of titanium chloride in the presence of nuclei of anatase TiO2 structure. Izv. Akad. Nauk SSSR, Neorgan. Mater. **24**: 1188–1191.
7. Pascual J, Camassel J and Mathieu H, 1977. Resolved quadrupolar transition in TiO_2. Phys. Rev. Lett. **39**: 1490–1493.

8. Kernazhitsky L, Shymanovska V, Naumov V, Chernyak V, Khalyavka T and Kshnyakin V, 2008. Effect of iron-group ions on UV absorption of TiO_2. Ukr. J. Phys. Opt. **9**: 197–207.
9. Anpo M, Aikawa N, Kubokawa Y, Che M, Louis C and Giamello E, 1985. Photoluminescence and photocatalytic activity of highly dispersed titanium oxide anchored onto porous Vycor glass. J. Phys. Chem. **89**: 5017–5021.
10. Amtout A and Leonelli R, 1995. Optical properties of rutile near its fundamental band gap. Phys. Rev**.** B. **51**: 6842–6851.
11. Ghosh A K, Wakim F G and Addiss R R, Jr, 1969. Photoelectronic processes in rutile. Phys. Rev. **184**: 979–988.
12. Khomenko V M, Langer K, Rager H and Fett A, 1998. Electronic absorption by Ti^{3+} ions and electron delocalization in synthetic blue rutile. Phys. Chem. Minerals. **25**: 338–346.
13. Jing L, Xin B, Yuan F, Xue L, Wang B and Fu H, 2006. Effects of surface oxygen vacancies on photophysical and photochemical processes of Zn-doped TiO_2 nanoparticles and their relationships. J. Phys. Chem. B. **110**: 17860–17865.
14. Serpone N, Lawless D, Disdier J and Herrmann J-M, 1994. Spectroscopic, photoconductivity, and photocatalytic studies of TiO_2 colloids – naked and with the lattice doped with Cr^{3+}, Fe^{3+}, and V^{5+} cations. Langmuir. **10**: 643–652.
15. Silva R C, Alves E and Cruz M M, 2002. Conductivity behaviour of Cr implanted TiO_2. Nucl. Instrum. Meth. B. **191**: 158–162.
16. Tang H, Berger H, Schmid P E and Levy F, 1994. Optical properties of anatase (TiO_2). Solid State Commun. **92**: 267–271.
17. Cardona M and Harbeke G, 1965. Optical properties and band structure of wurtzite-type crystals and rutile. Phys. Rev. A. **137**: 1467–1476.
18. Hossain F M, Sheppard L, Nowotny J and Murch G E, 2008. Optical properties of anatase and rutile titanium dioxide: Ab initio calculations for pure and anion-doped material. J. Phys. Chem. Solids. **69**: 1820–1828.
19. Glassford K M and Chelikowsky J R, 1992. Structural and electronic properties of titanium dioxide. Phys. Rev. B. **46**: 1284–1298.
20. Hosaka N, Sekiya T, Satoko C and Kurita S, 1997. Optical properties of single-crystal anatase TiO_2. J. Phys. Soc. Japan. **66**: 877–880.
21. Asahi R, Taga Y, Mannstadt W and Freeman A J, 2000. Electronic and optical properties of anatase TiO_2. Phys. Rev. B. **61**: 7459–7465.
22. Praliaud H, Kodratoff Y, Coudurier G and Mathieu M V, 1974. Molecular spectrometric studies of complexes copper-pyridine catalysts of the oxidative coupling of phenols – I. Electronic and EPR studies of the catalytic complex. Spectrochim. Acta A. **30**: 1389–1398.
23. Tauc J, in: F Abeles (Ed.), Optical properties of solids (North-Holland, Amsterdam, 1972).
24. Pascual J, Camassel J and Mathieu H, 1978. Fine structure in the intrinsic absorption edge of TiO_2. Phys. Rev. B. **18**: 5606–5614.
25. Daude N, Gout C and Jouanin C, 1977. Electronic band structure of titanium dioxide. Phys. Rev. B. **15**: 3229–3235.
26. Bak T, Nowotny J, Rekas M and Sorrell C C, 2003. Defect chemistry and semiconducting properties of titanium dioxide: I. Intrinsic electronic equilibrium. J. Phys. Chem. Solids. **64**: 1043–1056.
27. Karvinen S, Hirva P and Pakkanen T A, 2003. Ab initio quantum chemical studies of cluster models for doped anatase and rutile TiO_2. J. Mol. Struct.: Theochem. **626**: 271–277.

28. Mo S D and Ching W Y, 1995. Electronic and optical properties of three phases of titanium dioxide: rutile, anatase, and brookite. Phys. Rev. B. **51**: 13023–13032.
29. Wang X H., Li J G, Kamiyama H, Katada M, Ohashi N, Moriyoshi Y and Ishigaki T, 2005. Pyrogenic iron(III)-doped TiO_2 nanopowders synthesized in RF thermal plasma: phase formation, defect structure, band gap, and magnetic properties. J. Am. Chem. Soc. **127**: 10982–10990.
30. Frova A, Body P J and Chen Y S, 1967. Electromodulation of the optical constants of rutile in the UV. Phys. Rev. **157:** 700–708.
31. Zhao X K and Fendler J H, 1991. Size quantization in semiconductor particulate films. J. Phys. Chem. **95**: 3716–3723.
32. Choudhury B and Choudhury A, 2012. Dopant induced changes in structural and optical properties of Cr^{3+} doped TiO_2 nanoparticles. Mater. Chem. Phys. **132**: 1112–1118.

Kernazhitsky L., Shymanovska V., Gavrilko T., Naumov V. and Kshnyakin V., 2013. Optical absorption of polydisperse TiO_2: Effect of surface doping by transition metal cations. Ukr.J.Phys.Opt. **14**: 15 – 23.

Анотація. *Досліджено вплив домішок іонів перехідних металів Cu, Fe, Co і Cr на оптичні спектри поглинання полідисперсних порошків нанокристалічного TiO_2 – рутилу і анатазу, синтезованих за ідентичних умов експерименту. Для всіх досліджених зразків рутилу спектрального зсуву краю оптичного поглинання не спостерігали, тоді як для зразків анатазу, модифікованих іонами Fe і Cr, зареєстровано „червоний" зсув краю поглинання. Ширина забороненої зони модифікованого рутилу практично не змінювалася. Водночас ширина забороненої зони модифікованого анатазу зменшувалась, а найбільше – для зразків A/Cr і A/Fe.*